

1  
2  
3  
4  
5  
6  
7  
8  
9  
10  
11  
12  
13  
14  
15  
16  
17  
18  
19  
20  
21  
22  
23  
24

Geochemistry, Geophysics, Geosystems

Supporting Information for

**Phosphorites, Co-rich Mn nodules, and Fe-Mn crusts from Galicia Bank, NE**

**Atlantic: Reflections of Cenozoic tectonics and paleoceanography**

<sup>1</sup> Geological Survey of Spain (IGME), C/ Ríos Rosas 23, 28003 Madrid, Spain

<sup>2</sup> U. S. Geological Survey (USGS), Pacific Coastal and Marine Science Center, Santa Cruz, CA, United States

<sup>3</sup> Estación de Bioloxía Mariña da Graña, Universidade de Santiago de Compostela, Rúa da Ribeira 1–4 (A Graña), 15590 Ferrol, Spain

\*Corresponding Author: F.J. González, Geological Survey of Spain (IGME), C/Ríos Rosas 23, 28003 Madrid, Spain. (fj.gonzalez@igme.es)

**Contents of this file**

**Text S1 to S5**  
**Figures S1 to S3**  
**Tables S1 to S3**

**Introduction**

25 This supporting information provides a general description of samples recovered and Lab  
26 methods (geophysics, mineralogy and geochemistry); supplementary information of  
27 geological setting and additional figures of seismic profiles in the studied area; XRD  
28 mineralogical data and diffractograms and EPMA geochemical analysis of mineral phases  
29 in phosphorites and ferromanganese deposits.

30

31 **Text S1.**

32 **1. Data and methods**

33

34 *1.1. Bathymetry and seismic reflection data*

35

36 MHRs profiles were collected using an array of five GI-guns© (two of 45 ci,  
37 two of 13 ci, and one of 24 ci) with a total volume of 140 ci. The GI-guns© were  
38 fired at a shot-spacing of 25 m, corresponding approximately every 10 s and  
39 recording 8 s. Data were received using a high-resolution seismic data acquisition  
40 system. The total active streamer was 600 m, consisting of 72 channels. The  
41 average penetration reached by the acoustic signal was about 2.5 s two-way travel  
42 time (TWTT). The MBES data were collected with the hull-mounted Simrad EM-  
43 12 dual echosounder system, which collected bathymetric and backscatter data.  
44 The MBES operated at a frequency of 12/13 kHz at a ping rate of 10 s. It has a fan  
45 width of 150° consisting of 162 beams of 1.8°/3.5° each. Our bathymetric data were  
46 combined with those obtained for the mapping of the Exclusive Economic Zone  
47 (ZEEE) of Spain in the area of the Galicia margin, collected from 2001 to 2005.

48 In order to constrain the age of episodes of mineralization that occurred in  
49 the region of Galicia Bank, we carried out a seismo-stratigraphic analysis of high-

50 resolution multichannel seismic data to identify major regional discontinuities.  
51 This task ties in to previous studies on Mesozoic-Cenozoic stratigraphy, magnetic  
52 anomalies, and seismo-stratigraphic architecture determined for Galicia Bank and  
53 along the adjacent continental margins of the northern Iberian Peninsula (Groupe  
54 [Galicia, 1979](#); Mauffret and Montadert, 1988; Murillas et al., 1990; Cande and  
55 Kent, 1992; Sibuet, 1992; Thinon, 1999; Vázquez et al., 2008; Ercilla et al., 2011).

56

### 57 *1.2. Sample analyses techniques*

58

59 Dredge (2 m by 0.8 m) hauls recovered slabs of white phosphorite  
60 impregnated with black Fe-Mn oxides, black Mn nodules, Fe-rich reddish nodules,  
61 and several fragments of igneous, metamorphic, and sedimentary rocks from  
62 basement outcrops and ice-rafted drop stones. In addition, a large collection of  
63 living and dead cold-water Scleractinia corals (*Lophelia Pertusa*, *Madrepora*  
64 *Occulata*) and other encrusting organisms was recovered (Somoza et al., 2014).  
65 Large slabs of phosphorite (<1m in maximum dimension) were collected at four  
66 stations: DRR36, DRR38, DRR47 and DRR81 (**Fig. 2**). Individual samples range  
67 from a few grams for nodules to ≈100 kg for large pavement-like slabs. Fe-Mn  
68 nodules and crusts were collected at nine stations: DRR-20, DRR21, DRR25,  
69 DRR36, DRR37, DRR38, DRR41, DRR47, DRR81 and DRR91 (**Fig. 2**). Thin Fe-  
70 Mn crusts coat all the hard substrates present in the area (basement rocks, drop  
71 stones, phosphorite slabs and nodules, and Fe-Mn deposits). Fe-Mn patinas,  
72 impregnations, and breccias of variable centimetre thicknesses occur on the  
73 surface and underside surface of many phosphorite slabs from stations DRR47 and

74 **DRR81 (Fig. 2). Previously MBES backscatter data and MHRS profiles indicated**  
75 **the presence of these deposits.**

76 **Analyses were carried out in the Central Labs of the Geological Survey of**  
77 **Spain (IGME), the Pacific Coastal and Marine Science Center of the United States**  
78 **Geological Survey (USGS), the “CAI de Geocronología y Geoquímica Isotópica”,**  
79 **and the “Centro Nacional de Microscopía Electrónica” at the Complutense**  
80 **University of Madrid (UCM).**

81 **Thin and polished sections of phosphorite and Fe-Mn nodules and crusts**  
82 **were prepared and studied under the petrographic and electron (SEM-EPMA)**  
83 **microscopes. Bulk mineralogical X-ray powder diffraction (XRD) profiles from 2θ**  
84 **2–60° in 0.005 steps were obtained for 21 sub-samples using XPERT PRO of**  
85 **PANalytical, Cu-Kα radiation (40 kV and 40 mA) with graphite monochromator,**  
86 **High Score software and ICDD data base. Samples for EPMA analysis were**  
87 **selected based on the microscopic observations to represent all the mineral deposit**  
88 **types. Analyses were conducted using a JEOL Superprobe JXA-8900 M, operating**  
89 **at 15–20 kV and 50 mA, fitted with wavelength dispersive spectrometers (WDS).**  
90 **Back-scattered electron images were also obtained with this instrument. Profiles**  
91 **across nodular samples were obtained to check the presence of compositional**  
92 **zoning. Standards included pure metals, synthetic and natural minerals, all from**  
93 **international suppliers. Sub-millimetre ferromanganese laminae of vernadite that**  
94 **encrusts phosphorite slabs and nodules were analysed using EPMA for samples**  
95 **DRR38-2 and DRR81-5. In addition, the external margin (vernadite patina) of Co-**  
96 **rich manganese nodule DRR81-1 and Fe-rich nodule DRR38-8 were studied by**  
97 **EPMA.**

98           **The Fe-Mn crusts and phosphorite slabs were separated into distinct layers**  
99 **and textural types (massive, laminated and brecciated) for chemical and**  
100 **mineralogical analyses. Major and trace elements contents of bulk samples were**  
101 **analysed by X-ray fluorescence (XRF) using a MagiX of PANalytical instrument**  
102 **with Rh radiation, and by induction coupled plasma atomic emission spectrometry**  
103 **(ICP-AES) respectively. Au and Na were measured using a VARIAN FS-220**  
104 **atomic absorption spectrometre. Accuracy of the data was checked by using**  
105 **international standard reference materials, and precision based on duplicate**  
106 **samples was found to be better than  $\pm 5\%$ .**

107           **Loss on ignition (LOI) was determined by calcination at 950 °C and S was**  
108 **measured using ELTRA CS-800 equipment. REY concentrations of selected**  
109 **samples were determined by ICP mass spectrometry (ICP-MS) using an Agilent**  
110 **7500 ce instrument. The standard reference materials SO-1 (CCMET), GSP-1**  
111 **(USGS) and BCR-1 (USGS) were used to test the analytical procedure for REY**  
112 **determinations. The accuracy and precision obtained were better than 10% for all**  
113 **REY. REY were normalised to shale (Post-Archean Australian Shale, PAAS;**  
114 **McLennan, 1989) for plotting. The Ce anomaly ( $Ce^*$ ) was calculated as  $Ce^* = \text{Log}$**   
115 **( $Ce/(2/3La+1/3Nd)$ ), all values normalised to PAAS. The Pearson product moment**  
116 **correlation coefficient was used to produce correlation matrices.**

117           **Sr isotopic analyses are used to constraint the timing of phosphogenesis and**  
118 **the history of mineralization fluids in the Galicia Bank region. Nd isotopes were**  
119 **also measured to determine the source of the mineralization fluids. The isotopic**  
120 **analyses were based on bulk mineralized samples, micro-drilling of selected parts,**  
121 **and leaching experiments (Table 3). All samples were dried to constant weight and**  
122 **ground to 160 mesh. The bulk samples were digested in HCl–HNO<sub>3</sub>–HF mixture to**

123 allow analysis of the bulk sample. Details of protocols of sample preparation are  
124 given in Galindo et al. (1994) and Darbyshire and Shepherd (1994). The leaching  
125 procedure uses 5 ml of 2.5N HCl for 20 min to obtain the carbonate fraction. After  
126 leaching, the dissolutions were centrifuged at 4000 rpm for 10 min, and then the  
127 supernatant was decanted and evaporated.

128 For Sr isotope ratio analyses, Sr was separated from the samples using  
129 standard ion exchange techniques detailed in Galindo et al. (1994). Sr isotope ratio  
130 measurements were made on a automate collector Phoenix TIMS mass  
131 spectrometer with 9 collectors at the Center of Geochronology and Isotopic  
132 Geochemistry of the Complutense University of Madrid. Reproducibility and  
133 accuracy of Sr isotope runs were checked periodically by running the Standard  
134 Reference Material NBS 987 along with the samples, with a mean  $^{87}\text{Sr}/^{86}\text{Sr}$  value of  
135  $0.710240 \pm 0.00001$  ( $2\sigma$  external standard deviation,  $n=14$ ). The Sr isotopic ratios  
136 were normalized to  $^{86}\text{Sr}/^{88}\text{Sr}=0.1194$ .

137 Reproducibility and accuracy of Nd isotope runs were checked periodically  
138 by running the Standard Reference Material LaJolla along with the samples, with  
139 a mean  $^{143}\text{Nd}/^{144}\text{Nd}$  value of  $0.511848 \pm 0.000003$  ( $2\sigma$  external standard deviation,  
140  $n=27$ ). The Nd isotopic ratios were normalized to  $^{146}\text{Nd}/^{144}\text{Nd}=0.7219$ .  
141 Reproducibility of Sr and Nd isotopic measurements was determined by repeat  
142 analysis of samples and standards, which show analytical errors of 0.01% for  
143  $^{87}\text{Sr}/^{86}\text{Sr}$  and 0.006% for  $^{143}\text{Nd}/^{144}\text{Nd}$  of the standard deviation.  $\epsilon_{\text{Nd}(t)} =$   
144  $((^{143}\text{Nd}/^{144}\text{Nd})_{\text{sample}} / (^{143}\text{Nd}/^{144}\text{Nd})_{\text{CHUR}} - 1) * 10,000$ , where CHUR (Chondritic  
145 Uniform Reservoir) is equivalent to the bulk Earth  $^{143}\text{Nd}/^{144}\text{Nd}$  ratio or  $\sim 0.512638$   
146 (DePaolo and Wasserburg, 1976).  $\epsilon_{\text{Nd}(t)}$  was calculated using  $^{147}\text{Sm}/^{144}\text{Nd}/_{\text{CHUR}(0)} =$   
147 0.115.

148

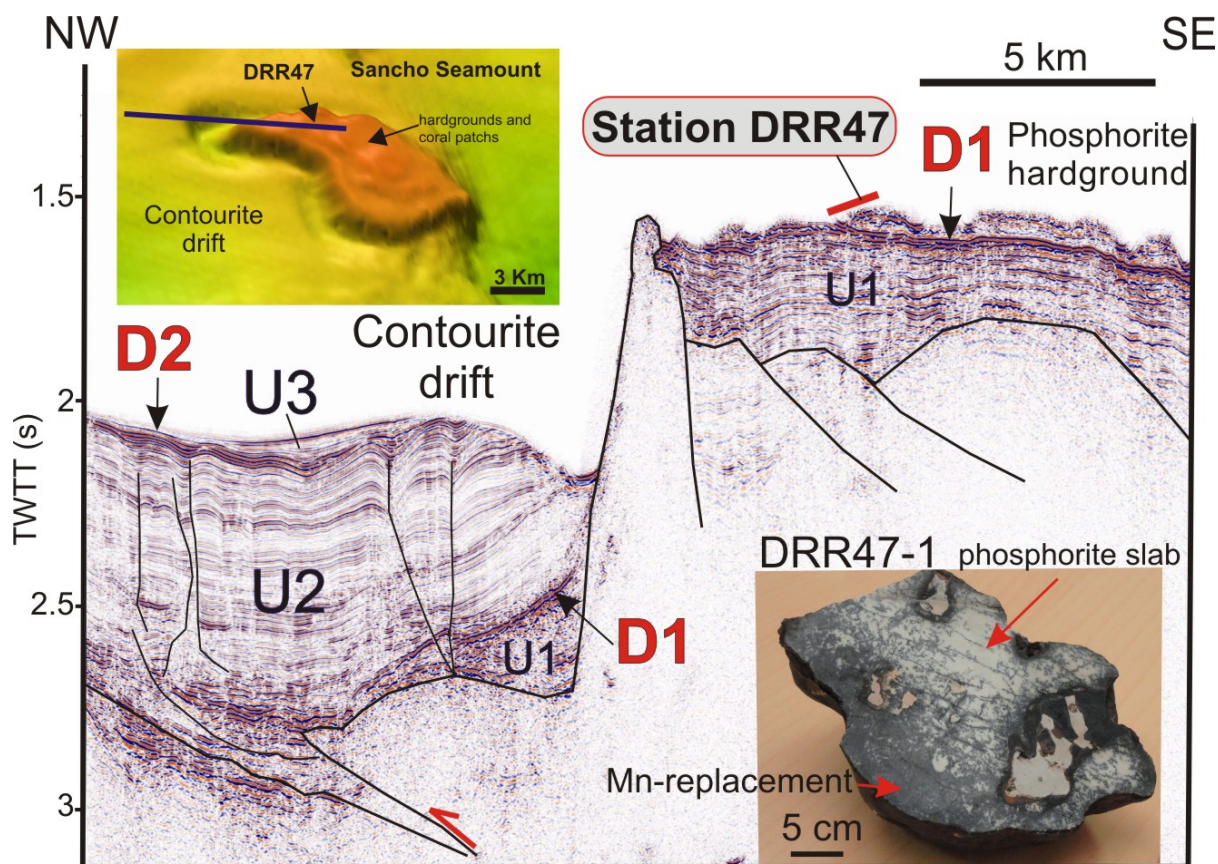
149 **Text S2.**

150 **2. Geological setting**

151 **Galicia Bank is bordered by two different margins (e.g. Boillot et al., 1989):**  
152 **(1) to the west, a passive rifted margin that resulted from the extension and**  
153 **breakup between America and Iberia during the Early Cretaceous. Samples**  
154 **recovered from the basement of the Galicia margin, especially at the fault scarps**  
155 **where basement crops out, reveal the nature of that margin. Metamorphic and**  
156 **plutonic rocks belong to two Variscan zones defined for on-land deposits**  
157 **(Capdevila and Mougnot, 1988). Tonalites and granodiorites, commonly found in**  
158 **the Ossa Morena zone, have been collected from Galicia Bank, Vasco de Gama and**  
159 **Vigo seamounts. Amphibolite, eclogite, gneiss, high-pressure granulite, and granite**  
160 **sampled along the northern Galicia margin belong to the Central Iberian Zone; (2)**  
161 **north of Galicia Bank occurs a Paleogene active margin. There, short-duration,**  
162 **latest Mesozoic-Early Cenozoic convergence between the Iberian and European**  
163 **plates transformed a Cretaceous passive margin into an active margin related to**  
164 **the southward subduction of the ocean lithosphere (Boillot and Mallod, 1988). The**  
165 **accretionary prism produced by this subduction appears to have been actively**  
166 **forming at least during Lutetian (middle Eocene) to Burdigalian (early Miocene)**  
167 **times (Alvarez-Marrón et al. 1997). Thus, the northwestern slope of Galicia Bank**  
168 **is composed of outcrops of mafic igneous rocks (basalts and gabbros) and**  
169 **peridotites (lherzolites, metasomatized peridotites, harzburgites) (Boillot et al.,**  
170 **1980; Cornen et al., 1999; Chazot et al., 2005). This zone has been interpreted as**  
171 **the margin of oceanic lithosphere accreted to the Iberian plate as a result of**  
172 **Cenozoic subduction. (Malod et al., 1993) and exhumed sub-continental**

173 lithospheric mantle respectively (e.g. Boillot et al., 1988). Syn- and post-rift  
 174 hydrothermal activity at shallow levels of the lithosphere has been proposed to  
 175 explain the serpentinization of peridotite (e.g. Boillot et al., 1989).

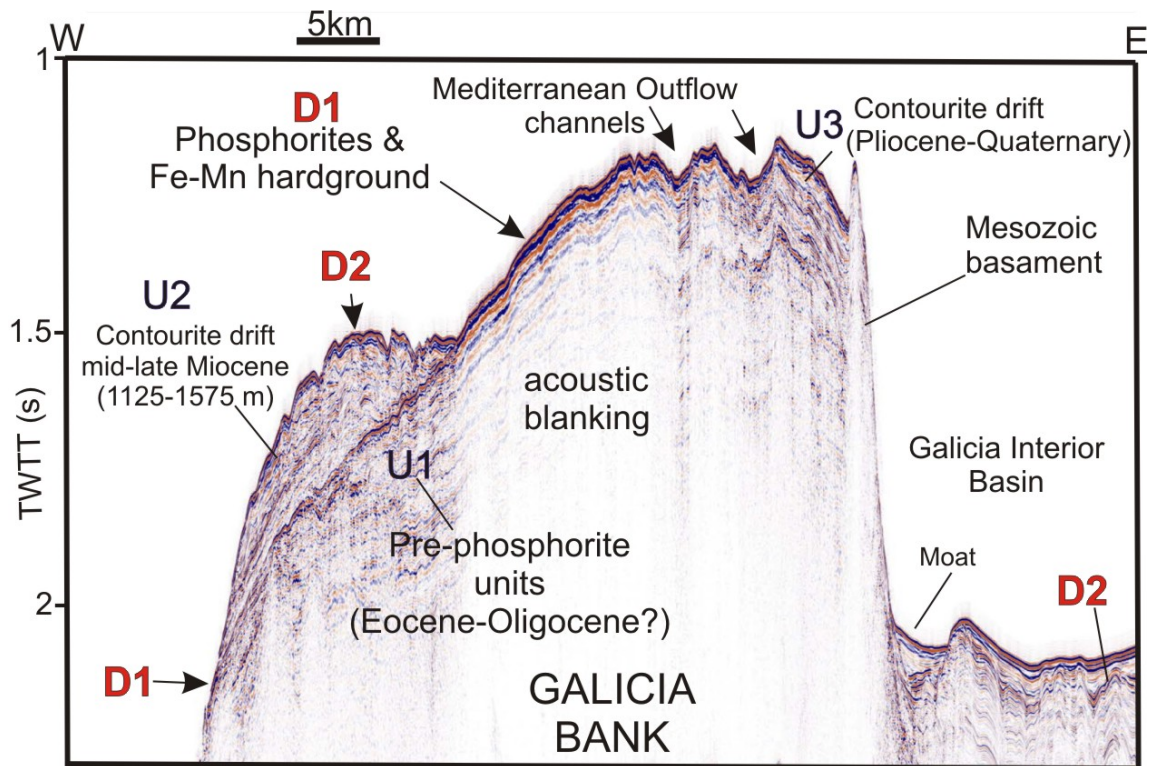
176  
 177  
 178



179  
 180 **Figure S1. NW-SE A04 multichannel seismic profile across the base and the Sancho**  
 181 **Seamount. Vertical exaggeration is x8 ( $V = 2.0\text{Km/s}$ ). Upper left is the location of seismic**  
 182 **profile and dredge station. A large suite of phosphorite slabs were collected from the top**  
 183 **of the seamount linked to the D1 discontinuity. Below on the right, phosphorite slab**  
 184 **showing a set of parallel fractures and partially replaced by Mn oxides (black) around the**  
 185 **margins and along fractures; pale-brown carbonate sediments fill cavities that were first**  
 186 **lined by Mn oxide.**

187

188  
189  
190  
191  
192



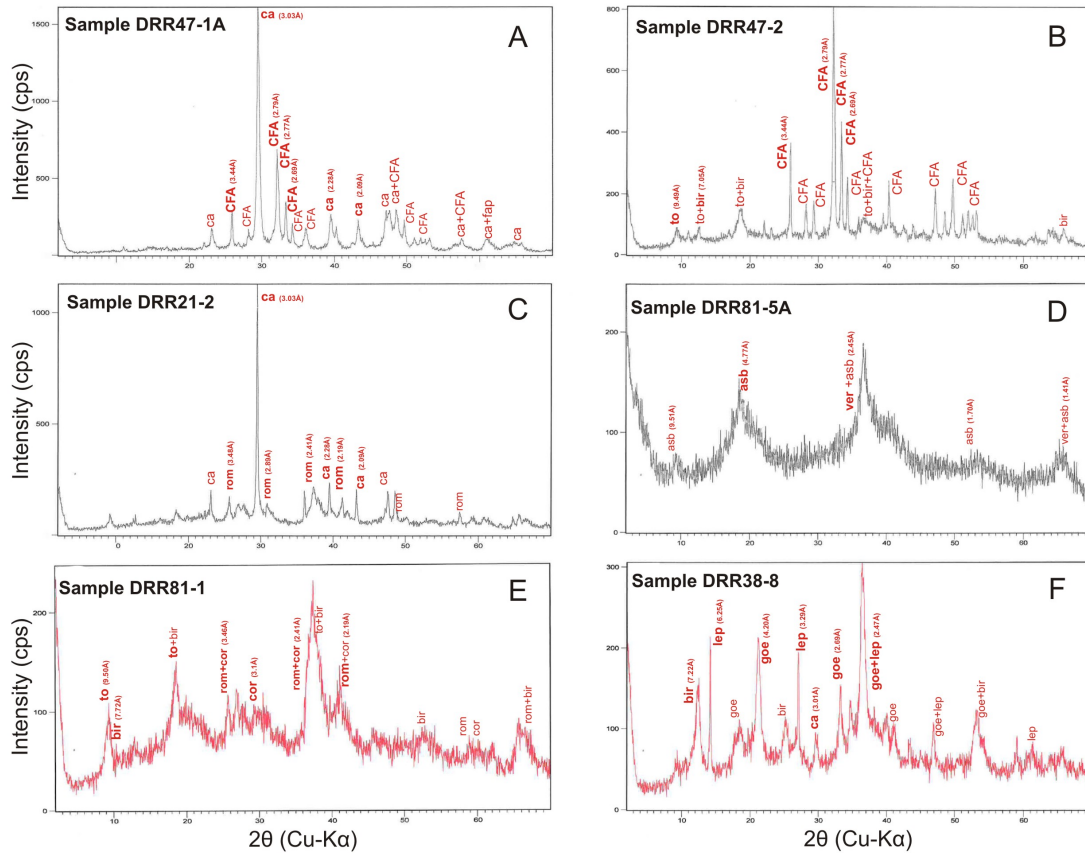
193  
194  
195  
196  
197  
198  
199  
200  
201  
202  
203

**Figure S2.** W-E A24 multichannel seismic profile across southern Galicia Bank (see Fig. 2). Vertical exaggeration is x32 ( $V = 2.0\text{Km/s}$ ). Mineral deposition can be associated with the seismic stratigraphy: Type 1, phosphorite hardground marks the D1 discontinuity; Type 2, hydrogenetic Fe-Mn crusts are associated with the U2 contourite unit; Type 3, Co-rich Mn nodules and Fe-Mn replaced phosphorite are linked to acoustic blanking related to upflow zones of fluids and sediment; Type 4, Fe-rich nodules are associated with contourites formed by the MOW.

**Text S3.**

### 3. Mineralogy

204           The XRD patterns of bulk samples and EPMA analyses show fluorapatite  
205 as the primary mineral and carbonate CFA as accessory (**Figs.S3A and B**).  
206 Fluorapatite has three main X-ray reflections at 2.79 Å, 2.69 Å and 2.77 Å. The  
207 crystallite size must be large as indicated by the sharp X-ray reflections on the  
208 XRD patterns. We cannot distinguish crystal morphologies, but the XRD patterns  
209 show resolved peaks reflecting moderate to high crystallinity of the phosphate  
210 mineral phases. Pyrite was not detected in the phosphate slabs or nodules.  
211 With respect to ferromanganese oxides, vernadite has two X-ray reflections at 2.45  
212 Å and 1.41 Å in Fe-Mn crusts. Asbolane has X-ray reflections at 4.81Å, 2.45 Å, 9.6  
213 Å, 1.71 Å and 1.41 Å (**Fig. S3D**). The XRD patterns of bulk Co-rich nodules show  
214 10 Å manganates as predominant: romanechite as the primary Mn mineral and  
215 coronadite and todorokite as accessories (**Figs. S3C and E** ). Goethite has two X-  
216 ray reflections at 2.47 Å and 4.20 Å being the principal mineral in Fe-rich nodules  
217 followed by lepidocrocite (**Fig. S3F**).



218

219 **Figure S3. XRD profiles for (A) phosphorite; (B) brecciated and Fe-Mn replaced**  
 220 **phosphorite that replaced limestone; (C, E) Co-rich Mn nodule; (D) hydrogenetic Fe-Mn**  
 221 **crust; (F) Fe-rich nodule. ca=calcite, CFA=carbonate fluorapatite, to=todorokite,**  
 222 **bi=birnesite, rom=romanechite, ver=vernadite, asb=asbolane, cor=coronadite,**  
 223 **goe=goethite, lep=lepidocrocite.**

224

225 **Text S4.**

226 **4. Electron Micro Probe Analysis and Pearson correlation Index**

227

228 **For six samples of phosphorites, P has a positive correlation with F (0.82)**  
 229 **and Na (0.8) (Table S1). The terrigenous elements Si, Al, Mg, K and Ti show**  
 230 **positive correlations among members of that group (0.8-0.9). Fe exhibits a positive**  
 231 **correlation with Mn (0.86) and a negative correlation with Ca (-0.93). Ca shows a**  
 232 **negative correlation with Mn (-0.96) and Mg (-0.86).**

233           **Microprobe analyses of phosphate minerals in slabs and nodules show that**  
234 **CFA in slabs significantly concentrates F (up to 4.1 wt%), CaO (48.2 to 53.2 wt%),**  
235 **P<sub>2</sub>O<sub>5</sub> (29.8 to 34.3 wt%), and SO<sub>3</sub> (up to 1.4 wt%; **Table S2**). Phosphorite slabs**  
236 **showing replacement by Fe-Mn oxyhydroxides have characteristic geochemical**  
237 **zonations: Fe and Mn are strongly enriched in the replaced margins compared to**  
238 **the unaltered phosphorite slabs (up to 49.7 wt% MnO and 7.8 wt% FeO); Sr, Ba,**  
239 **Ni, Co and Pb are also enriched along with the Mn and Fe, but P<sub>2</sub>O<sub>5</sub> contents are**  
240 **lower (**Table S2**, analyses DRR47-2-(3, 4, 12)). Phosphate nodules have P<sub>2</sub>O<sub>5</sub>**  
241 **contents that are slightly lower than the phosphorite slabs (from 27.2 to 30.3 wt%),**  
242 **and the nodules show higher contents in FeO (up to 5.3 wt%) and MnO (up to 5.8**  
243 **wt%).**

244           **Elements in the Fe-Mn deposits are associated with different mineral**  
245 **phases: vernadite, goethite, 7 Å and 10 Å manganates, aluminosilicates, biogenic**  
246 **carbonate clasts or carbonates filling porosity, Mn-carbonates, and CFA.**  
247 **Microprobe point analyses of vernadite, which encrusts the surface of Fe-Mn**  
248 **nodules and phosphates, show variable contents of major, minor and trace metals**  
249 **among different samples but also among laminations in the same sample (**Table****  
250 **S3**). For vernadite, Mn/Fe ratios are close to 1 with high Co contents (up to 1.3  
251 wt%) and Pb (up to 0.67 wt%) and minor Ni. In other samples, Mn/Fe ratios are  
252 higher (up to 500) accompanied by Ni contents (up to 3 wt%) and Cu contents (up  
253 to 0.3 wt%). The 7 Å and 10 Å manganates in the Co-rich Mn nodules, such as  
254 DRR81-1, concentrate Mn (up to 60.7 wt% MnO), with high contents in Mg, Ca,  
255 Na, and K, and also elements of potential economic interest: Co (up to 5.6 wt%),  
256 Ba (up to 6.6 wt%), Ni (up to 1.2 wt%), and Cu (up to 0.2 wt%). Mn-carbonate  
257 laminae in these nodules concentrate Ca, Mn, Mg, Co and P. The goethite in Fe-

258 rich nodules concentrates only Fe (up to 75 wt% FeO), with low concentrations of  
259 other metals. Detrital phyllosilicates host Al, Si and K and frequently also Fe and  
260 Mg, whereas bioclasts in phosphorite and Fe-Mn nodule content show high Ca, Mg  
261 and Sr.

262

263 **Text S5.**

## 264 **5. References**

265 Boillot, G., Grimaud, S., Mauffret, A., Mougnot, D., Kornprobst, J., Mergoill-  
266 Daniel, J., and G. Torrent (1980), Ocean-Continent Boundary Off the Iberian  
267 Margin: a Serpentinite Diapir West of the Galicia Bank. *Earth Planet. Sci. Lett.*,  
268 48(1), 23-34.

269 Boillot, G., Mougnot, D., Girardeau, J., and E. L. Winterer (1989), Rifting  
270 Processes on the West Galicia Margin, Spain. In: A.J. Tankard and H.R. Balkwill  
271 (Eds.) *Extensional Tectonics and Stratigraphy of the North Atlantic Margins.*  
272 *AAPG Memoir 46*, 363-377.

273 Chazot, G., Charpentier, S., Kornprobst, J., Vannucci, R., and B. Luais (2005),  
274 Lithospheric Mantle Evolution during continental Break-Up: The West Iberia Non-  
275 Volcanic Passive Margin. *J. Petrol.*, 46 (12), 2527-2568.

276 Cornen, G., Girardeau, J., and C. Monnier (1999), Basalts, underplated gabbros  
277 and pyroxenites record the rifting process of the West Iberian margin. *Min. and*  
278 *Petrol.*, 67, 111-142

279 Darbyshire, D. P. F., and T. J. Shepherd (1985), Nd and Sr isotope constraints on  
280 the origin of the Cornubian Batholith, SW England. *J. Geol. Soc. London*, 142,  
281 1159-1177.

282 DePaolo, D.J., and G.J. Wasserburg (1976), Nd isotopic variations and  
283 petrogenetic models, *Geophys. Res. Lett.*, 3, 249-252.

284 Ercilla, G., Casas, D., Vázquez, J.T., Iglesias, J., Somoza, L., Juan, C., Medialdea,  
285 T., León, R., Estrada, F., García-Gil, S., Farrán, M., Bohoyo, F., García, M., and  
286 A. Maestro (2011), Imaging the recent sediment dynamics of the Galicia Bank  
287 region (Atlantic, NW Iberian Peninsula). *Mar. Geoph. Res.*, 32 I, 1–2, 99–126.

288 Galindo, C., Tornos, F., Darbyshire, D. P. F., and C. Casquet (1994), Sm/Nd dating  
289 and isotope constraints for the origin of the barite-fluorite (Pb-Zn) veins of the  
290 Sierra del Guadarrama (Spanish Central System, Spain). *Chem. Geol.*, 112 (3-4),  
291 351-364.

292 Groupe Galicia (1979), The continental margin off Galicia and Portugal: acoustical  
293 stratigraphy, dredge stratigraphy and structural evolution. In: Sibuet JC, et al.  
294 (Ed.), *Init. Rep. DSDP 47*. U.S. Government printing Office, Washington D.C., 633–  
295 662

296 Malod, J. A., Murillas, J., Kornprobst, J., and G. Boillot (1993), Oceanic  
297 lithosphere at the edge of a Cenozoic active continental margin (northwestern  
298 slope of Galicia Bank, Spain). *Tectonophysics*, 221, 195-206.

299 Mauffret, A., and L. Montadert (1988), Seismic stratigraphy off Galicia. In:  
300 Boillot, G., Winterer, E.L., et al. (Eds). *Proc. ODP. Sci. Results*, 103: 13–30.

301 Murillas, J., Mougnot, D., Boillot, G., Comas, M. C., Banda E., and A. Mauffret  
302 (1990), Structure and evolution of the Galicia Interior Basin (Atlantic western  
303 Iberian continental margin). *Tectonophysics*, 184, 297-319.

304 **Cande, S. and D. Kent (1992), A new geomagnetic polarity time scale for the late**  
305 **Cretaceous and Cenozoic, *J. Geophys. Res.*, 97, 13917-13951.**

306 **Somoza, L., Ercilla, G., Urgorri, V., León, R., Medialdea, T., Paredes, M.,**  
307 **González, F. J., and M. A. Nombela (2014), Detection and mapping of cold-water**  
308 **coral mounds and living *Lophelia* reefs in the Galicia Bank, Atlantic NW Iberia**  
309 **margin. *Mar. Geol.*, 349, 73-90.**

310 **Sibuet, J. C. (1992), New Constraints on the formation of the nonvolcanic**  
311 **continental Galicia-Flemish Cap conjugate margins. *J. Geol. Soc.*, 149, 829-840.**

312 **Thinon, I. (1999), Structure profonde de la Marge Nord Gascogne et du Bassin**  
313 **Armoricain, Université de Bretagne Occidentale, Brest, 327 pp.**

314 **Vázquez, J.T., Medialdea, T., Ercilla, G., Somoza, L., Estrada, F., Fernández-**  
315 **Puga, M.C., Gallart, J., Gràcia, E., Maestro, A., and M. Sayago (2008), Cenozoic**  
316 **deformational structures on the Galicia Bank Region (NW Iberian continental**  
317 **margin). *Mar. Geol.*, 249 (1-2), 128-149.**